Mukhopadhyay, S., & Hallett, S. (2019). A directed continuum damage mechanics method for modelling composite matrix cracks. *Composites Science and Technology*, *176*, 1-8. https://doi.org/10.1016/j.compscitech.2019.03.022

A directed continuum damage mechanics method for modelling composite matrix cracks

Supratik Mukhopadhyay*, Stephen R. Hallett

University of Bristol, Advanced Composites Collaboration for Innovation and Science, Queens Building, Bristol BS8 1TR, United Kingdom

*Corresponding author. Email: email.supratik@gmail.com

Abstract

Matrix cracking in continuous fibre reinforced composites follows the fibre orientations, but continuum damage mechanics models are not able to properly capture this. A novel method is presented here to alleviate mesh sensitivity of the damage growth direction and represent discrete matrix cracks. In a ply-by-ply mesoscale model, matrix cracks within a ply usually rely on mesh dependent strain localisation to decide the crack growth direction. The newly proposed algorithm instead uses the ply level fibre orientation as a model input, and maintains crack advancement along this direction, based on a neighbour searching scheme. A further advantage is that it is able to represent individual cracks discretely, with a predefined minimum crack spacing. This overcomes another limitation of continuum damage models, where discrete cracks are only represented in a smeared sense. This procedure has been shown to be able to reproduce complex crack networks in multidirectional laminates, independent of the mesh pattern.

Keywords: A. Structural composites, B. Matrix cracking, C. Damage mechanics, C. Finite element analysis (FEA), Tracking algorithms

1 Introduction

Continuum damage mechanics (CDM) is a framework for modelling material failure as progressive loss of stiffness at the macroscale due to diffused damage occurring at the microscale such as coalesce and growth of microcracks, voids and other kinds of defects. The concept was first introduced by Kachanov [1] in the context of creep rupture, and was subsequently expanded by Rabotnov [2], Lecky and Hayhurst [3], Chaboche [4], Lemaitre[5] and many others. In its simplest isotropic version, a single non-decreasing scalar variable is used to represent the evolution of damage, by progressively reducing the material stiffness from its initial undamaged value to zero at complete failure. A more refined theory considers damage anisotropy in different material directions with the help of a damage tensor, whose components represent damage evolution in different directions. From the perspective of numerical implementation, continuum damage models are an attractive choice to model structural failure since the damage law can easily be incorporated in the form of a user defined material in any commercial finite element package. Due to this, several instances of development and application of these damage models can be found throughout the literature for application to continuous fibre reinforced laminated composites e.g. Ladeveze and Dantec [6], Pinho *et al*.[7,8], Maimí*et al*.[9–11], Williams and Vaziri [12], van der Meer and Sluys [13]to name just a few. In a mesomechanical approach, where a single ply within a laminate constitutes the smallest scale of analysis, traditionally single integration point elements are used to implement a CDM material law. In such a case, the stress vs. strain response of the integration point represents the response of the entire volume of the associated element, which implies that the damage response is 'smeared' over the element volume. Hence these formulations are also known as smeared damage laws.

Damage evolution in a CDM typically follows a strain-softening behaviour. A well-known numerical problem associated with a strain-softening constitutive behaviour is 'localisation'.

This indicates that damage always tends to localise in one row of finite elements. Hence with progressive mesh refinement, as the element dimension tends to zero, energy dissipation due to damage will also tend to zero, which is clearly non-physical. The reasons for strain localisation and its effects are discussed in Bazant and Belytschko[14] and Bazant and Oh[15,16].Several approaches have been proposed to overcome this problem and the most popularly used method in composite damage analysis is the crack band theory suggested in [15]. In a crack band approach, the element characteristic length of the finite element mesh is precomputed and explicitly included in the failure constitutive law (see the work by Maimi *et al*.[17] as an example). This guarantees regularised energy dissipation, independent of the mesh size. Although this approach is quite straightforward to implement, it does not address the underlying problem of strain localisation directly but instead masks it by the regularisation parameter. Another undesired consequence of the localisation problem, which is the subject of the present work, is spurious sensitivity of the damage growth direction along the mesh lines of the finite element model. This is particularly concerning when modelling intra-laminar matrix crack development within a laminate. Because laminates are usually constructed by stacking multiple plies with different fibre direction in each, the crack growth direction needs to follow the local fibre direction in each ply, and not the underlying mesh pattern. Although transverse matrix cracking is regarded as a secondary failure mode, being relatively benign on its own to cause global failure, there are several instances reported[18–20]where they strongly interact with inter-ply delaminations, resulting in a plane of delamination migrating to another weak ply interface and causing unexpected failure. In these cases, incorrectly predicted matrix crack paths will lead to an incorrect sequence of overall damage progression, and consequently an incorrect laminate strength. Therefore, in such cases it is extremely important to correctly capture the crack growth direction for reliable numerical predictions. Three approaches are generally used within the composites

community to address this problem. The first one is to design the mesh in each individual ply to be aligned with the local fibre direction, e.g. Nikishkov *et al*. [21], Song *et al*.[22], Lopez *et al*.[23]. Not only does this demand a considerable meshing effort, but also it is not always possible to satisfy this requirement while meshing complex 3D geometry. Most importantly, this results in non-matched mesh at the ply interfaces, which require tie constraints between the plies to hold the assembly together, or the use of contact based cohesive interface formulations, both of which significantly increase the computational time. Further, the ply mesh needs to be sufficiently fine to simulate discrete cracks, which are able to initiate and interact with delaminations. A variation of this approach without the use of a continuum damage model is to use cohesive elements to represent matrix cracks, which are pre-inserted between solid ply elements in the regions of interest in the mesh, following the fibre direction[24–27]. The second approach is to eliminate the problem of localisation altogether by using nonlocal averaging scheme, e.g. Forghani and Vaziri[28]. In this method, the local material pointwise strain is averaged over a region of finite radius using a Gaussian or bell-shaped power function (see Jirasek [29] for a comprehensive review of this method) and this nonlocal strain is used to construct the damage variable. Whilst this method successfully eliminates the mesh- pattern bias of the crack growth direction, it introduces an additional parameter, namely the averaging radius, which needs to be carefully selected. In the macro scale damage model implemented in [28], the averaging radius is determined by post processing images of failed test specimens to identify the width of the damaged region, which is taken to be a measure of this radius. This is not feasible in a ply-level analysis, where, matrix cracks within a ply are accompanied by extremely small process zones, owing to the brittle nature of the resin. The process zone in this scale of analysis is typically comparable to the order of individual element size of the FE mesh, and thus does not yield any computational advantage. Further, due to the averaging, damage does not appear as sharp

cracks in this method, but as a finite band spanning a few elements. This also results in poor interaction with cohesive interface elements between plies for initiating delamination. The third approach to solve the localisation problem is to model cracks using partition-of-unity based strong discontinuity modelling techniques, rather than continuum damage. This includes application of eXtended finite element method (XFEM)[30,31] and its variant regularised XFEM[32], Phantom Node Method (PNM)[33], Floating Node Method(FNM) [34], Augmented Finite Element Method (AFEM)[35,36], Cohesive Segment Method [37] and its variant [38] etc. This class of methods is not influenced by mesh-pattern dependence and by far are the most accurate in simulating realistic crack growth and interaction with delamination and other damage modes in composites. However, these are significantly computationally expensive compared to the other methods discussed above and are not straightforward to be implemented in commercial FE solvers. Further, these methods still lag behind standard continuum damage models in terms of robustness and scalability.

In the current work, we present a new technique that combines features of a standard continuum damage model and mesh-independent strong discontinuity model. It preserves the ease of implementation and robustness of CDM models for matrix cracking, while allowing the user to simulate multiple discrete cracks which are mesh-pattern independent. Crack initiation locations are a model outcome and are not needed to be specified a priory. As will be shown, this simple element-wise fibre tracking algorithm eliminates the mesh pattern bias. It is implemented in Abaqus/Explicit, but any other commercial FE software which supports user material subroutines is equally suited for this method. Examples are given in terms of models run on multiple CPUs in a high-performance Linux cluster, where multidirectional crack networks interact with delaminations, leading to failure.

2 Matrix crack model

2.1 Constitutive law

In this work, the 3DCDM law proposed by Pinho *et al*. [7] is used for matrix cracking. 8 node solid brick elements C3D8R with reduced integration in Abaqus [39] are used for the implementation. The damage law is briefly outlined below for completeness:

Referring to Figure 1(a), the material frame stresses are rotated to a hypothetical crack frame which is oriented at an angle φ (yet to be determined) with the ply normal:

$$\sigma_{\mathrm{N}} = \frac{\sigma_{22}-\sigma_{33}}{2} + \frac{\sigma_{22}-\sigma_{33}}{2}\cos 2\varphi + \tau_{23}\sin 2\varphi \tag{1}$$

$$\tau_{\mathrm{T}} = -\frac{\sigma_{22}-\sigma_{33}}{2}\sin 2\varphi + \tau_{23}\cos 2\varphi \tag{2}$$

$$\tau_{\mathrm{L}} = \tau_{12}\cos\varphi + \tau_{13}\sin\varphi \tag{3}$$

where σ_{N} is the normal stress while τ_{T} and $\tau_{\mathrm{L}}$are the two shear stress components on the crack frame.

Similarly, the normal strain ϵ_{N} and shear strains γ_{T} and γ_{L}on the crack frame are:

$$\epsilon_{\mathrm{N}} = \frac{\epsilon_{22}-\epsilon_{33}}{2} + \frac{\epsilon_{22}-\epsilon_{33}}{2}\cos 2\varphi + \gamma_{23}\sin 2\varphi \tag{4}$$

$$\gamma_{\mathrm{T}} = -\frac{\epsilon_{22}-\epsilon_{33}}{2}\sin 2\varphi + \gamma_{23}\cos 2\varphi \tag{5}$$

$$\gamma_{\mathrm{L}} = \gamma_{12}\cos\varphi + \gamma_{13}\sin\varphi \tag{6}$$

The crack frame orientation φ is found by the maximum of the failure criteria in equation (7)over possible fracture angles in the range 0° and 180°:

$$\left(\frac{\sigma_{\mathrm{N}}}{Y_{\mathrm{T}}}\right)^2 + \left(\frac{\tau_{\mathrm{L}}}{S_{\mathrm{L}}}\right)^2 + \left(\frac{\tau_{\mathrm{T}}}{S_{\mathrm{T}}}\right)^2 = 1;\ \ \sigma_{\mathrm{N}} \geq 0 \tag{7}$$

$$\left(\frac{\tau_{\mathrm{L}}}{S_{\mathrm{L}}-\mu_{\mathrm{L}}\sigma_{\mathrm{N}}}\right)^2 + \left(\frac{\tau_{\mathrm{T}}}{S_{\mathrm{T}}-\mu_{\mathrm{T}}\sigma_{\mathrm{N}}}\right)^2 = 1;\ \ \sigma_{\mathrm{N}} < 0 \tag{8}$$

whereY_{T} is the ply transverse tensile strength, S_{L} and S_{T} are the longitudinal and transverse shear strengths respectively. Similarly, friction coefficients on the crack plane in the longitudinal and transverse direction are$\mu_{\mathrm{L}}$and μ_{T}.S_{T} , μ_{T} and $\mu_{\mathrm{L}}$are obtained from the

transverse compressive strength Y_c and corresponding fracture angleφ(denoted by$\varphi_0$and is equal to 53˚) using Mohr-Coulomb theory:

$$S_T = \frac{Y_c}{2\tan\varphi_0}, \mu_T = -\frac{1}{\tan(2\varphi_0)}, \mu_L = S_L\frac{\mu_T}{S_T} \tag{9}$$

Once damage is initiated at a certain crack frameφ, an equivalent mixed-mode damage driving stress σ_m and displacement δ_m are ascertained:

$$\sigma_m = \sqrt{\langle\sigma_N\rangle^2 + (\tau_T)^2 + (\tau_L)^2} \tag{10}$$

$$\delta_m = \left(\frac{\langle\sigma_N\rangle\langle\epsilon_N\rangle + \tau_T\gamma_T + \tau_L\gamma_L}{\sigma_m}\right) l_e \tag{11}$$

In Equation (10) and (11), Macaulay bracket indicates that negative values of stresses and strains do not enter the constitutive equation, as they tend to close the crack rather than driving the damage further. The parameter l_e in Equation (11) is the characteristic element length. The default value of characteristic length accessible from the user material subroutine, which is given by the cube root of the element volume, is used in this work. This simplification is in keeping with the fact that all the elements in the fine mesh region of the models presented here (see Section 3) are nearly cuboidal and that the crack frame angle ,φ, is approximately equal to 0˚, since the tensile loading renders all elements either under pure transverse tension or under a combination of transverse tension/in-plane shear. For a more general three dimensional stress state, and for crack growth that is not orthogonal to the loading direction, a more accurate measure of the element characteristic length can be calculated as the ratio between the element volume and the cracked area within the element. The cracked area is a function of the ply orientation, element edge dimensions, crack frame angle φ and the crack's position within the element (obtained from the edge cut point coordinates, which are already obtained as part of the solution).

The mixed-mode critical energy release rate G_C for failure is determined following the power law criterion:

$$\left(\frac{G_{\mathrm{I}}}{G_{\mathrm{IC}}}\right)^{\alpha}+\left(\frac{G_{\mathrm{II}}}{G_{\mathrm{IIC}}}\right)^{\alpha}=1 \tag{12}$$

where $G_{\mathrm{I}}$and $G_{\mathrm{II}}$are the mode I and mode II energy release rates and the corresponding critical values attained under individual modes are denoted with suffix 'C'. The power law exponent is α. This leads to the following expression for G_{C}:

$$G_{\mathrm{C}}=\left[\left\{\frac{1}{G_{\mathrm{IC}}}\left(\frac{\langle\sigma_{\mathrm{N}}^{\mathrm{o}}\rangle\epsilon_{\mathrm{N}}^{\mathrm{o}}}{\sigma_{\mathrm{m}}^{\mathrm{o}}\epsilon_{\mathrm{m}}^{\mathrm{o}}}\right)\right\}^{\alpha}+\left\{\frac{1}{G_{\mathrm{IIC}}}\left(\frac{\tau_{\mathrm{T}}^{\mathrm{o}}\gamma_{\mathrm{T}}^{\mathrm{o}}+\tau_{\mathrm{L}}^{\mathrm{o}}\gamma_{\mathrm{L}}^{\mathrm{o}}}{\sigma_{\mathrm{m}}^{\mathrm{o}}\epsilon_{\mathrm{m}}^{\mathrm{o}}}\right)\right\}^{\alpha}\right]^{-\frac{1}{\alpha}} \tag{13}$$

In Equation (13), the prefix 'o' on a quantity indicates its value at damage onset. The relative displacement between the crack surfaces at failure $\delta_{\mathrm{m}}^{\mathrm{f}}$ (superscript 'f' indicates failure) can now be defined as:

$$\delta_{\mathrm{m}}^{\mathrm{f}}=\frac{2G_{\mathrm{c}}}{\sigma_{\mathrm{m}}^{\mathrm{o}}l_{e}} \tag{14}$$

A damage variable $d\in[0,1]$ is finally introduced which drives the damage:

$$d=\frac{\delta_{\mathrm{m}}^{\mathrm{f}}(\delta_{\mathrm{m}}-\delta_{\mathrm{m}}^{0})}{\delta_{\mathrm{m}}(\delta_{\mathrm{m}}^{\mathrm{f}}-\delta_{\mathrm{m}}^{0})} \tag{15}$$

This damage variable is then used to degrade the mixed-mode damage driving stress σ_{m}linearly to zero in subsequent increments (Figure 1(b)).

However, a straightforward implementation of the above-mentioned damage law leads to spurious mesh pattern bias, as already discussed in the introduction. A ply-level fibre tracking algorithm is thus introduced to alleviate this problem.

2.2 Fibre direction tracking

To make the crack growth independent of the mesh pattern, local fibre directions needs to be known during computation. This is achieved by reading a file at the start of the simulation, which is prepared in advance and contains information about element numbers, corresponding ply ids and ply fibre directions written down in a tabular format. This information is stored in state variables. Additionally, the mesh file is read at the beginning

and the element connectivity information is retrieved. For each element, this information is used to identify the four edge sharing neighbour elements in the same ply. The damage state of a given element (elastic/damaged/failed) is then passed to these four neighbours at each time increment until failure, which forms the basis of the tracking algorithm. Once the initiation criteria (equation (7) or (8)) is met in an element, a check is performed whether any of the adjoining four neighbours has already damaged/failed. If this is not the case, the path of the crack segment is assumed to traverse through the element integration point. The coordinates of this point together with the slope obtained from ply fibre angle uniquely defines the straight line crack segment within the element. To identify the element edges that are intercepted by this segment, a signed distance function$\varphi(\boldsymbol{x})$ is discretely evaluated at the two corner nodes of each edge:

$$\varphi(\boldsymbol{x}) = min_{\boldsymbol{x_c}\in\Gamma_c}\|\boldsymbol{x}-\boldsymbol{x_c}\|sign(\boldsymbol{n}.[\boldsymbol{x}-\boldsymbol{x_c}]) \tag{16}$$

where Γ_c denotes the crack segment and $\boldsymbol{n}$ is the crack normal. A cut edge results in $\varphi(\boldsymbol{x})$ to be evaluated to opposite signs at its two supporting nodes. Once the cut edges are identified, points of intersection of the element edges with the crack segment are obtained by solving straight line equations. These intersection points are passed to the neighbours sharing common cut edges as additional information. If a neighbour is found to be already damaged/failed, the crack segment then passes through the intersection point previously transferred to this element to maintain crack path continuity (figure 2(a) and (b)).

Because this method is still not a discrete crack model, the crack segments are not individually represented, but smeared over the element volume, thus an element-by-element propagation results. However, to preserve discreteness, for each new crack, damage is limited only to just one row of elements in the direction of crack growth. This is effected by artificially blocking initiation in a small user-defined circular region around the currently damaged element (Figure3) except for its immediately adjacent neighbours that are aligned

with the fibre direction. Once the crack advances, some of the 'blocked' elements are accordingly reactivated. As will be shown, this allows multiple parallel ply cracks to initiate in solution dependent locations and grow completely independent of the mesh and interact with inter-ply delaminations appropriately.

The exchange of data between elements during runtime needs special mention. In the actual implementation, this is done with the help of COMMON BLOCK variables within the FORTRAN programme, wherein information is stored globally and accessed from all the elements at runtime. However, the present modelling approach is aimed for large structural problems for which parallel processing (running on several CPUs simultaneously) is an essential requirement to limit computation to practical timescales. Usage of COMMON variables generally prohibits multi-CPU implementation as data stored in these variables are not properly communicated between participating CPUs or data is overwritten, producing unpredictable results. This hurdle has been overcome using the recently introduced VEXTERNALDB subroutine in Abaqus/Explicit 6.14 [39]which allows including MPI libraries in a multi-CPU environment and efficiently exchanging information between the CPUs, making it convenient to implement such non-local modelling schemes for a large number of elements.

3 Example cases

The method's performance is tested with two example problems, where matrix cracks interact with other damage mechanism, and therefore their accurate representation is important, as discussed below. Comparisons are also drawn with results obtained by running the same models with traditional CDM method.

3.1 Static tensile failure of open-hole quasi-isotropic laminate

Static tensile failure of open-hole quasi-isotropic laminate is a challenging problem [40]that has been used by many authors to verify modelling methods and their ability to accurately capture matrix crack-delamination interaction. Keeping the same model geometry, two different layups are investigated from existing literature: $[45_2/90_2/-45_2/0_2]_S$ [41] and $[90_2/-45_2/0_2/45_2]_S$ [42]. . The failure is by delamination in both cases, but differs significantly in terms of failure load. In the first $[45_2/90_2/-45_2/0_2]_S$ laminate case, the delamination is seen to initiate at the boundary of a 3.175 mm diameter hole and then propagate outwards while remaining confined between the bounds of plus and minus 45° ply matrix cracks, before propagating back to the grips at the -45/0 interface. This strong coupling between cracks and delamination results in triangular delamination patterns (Figure 4) on either side of the hole. Figure 5 shows the FE mesh of the laminate with the associated boundary conditions. A fine mesh with in-plane element size 0.25 mm×0.25 mm in the central region is used. Between every two plies (modelled using a single layer of solid C3D8R elements), a thin (0.01 mm) layer of cohesive COH3D8 elements are inserted to simulate delamination. Although the ply behaviour is modelled using the present user material formulation, the cohesive material model already existing in Abaqus is used for the cohesive elements. The ply and cohesive interface material properties used in the present study are listed in Table 1 and Table 2 respectively.

Due to symmetry in the z direction, only half of the laminate is modelled and z-symmetry boundary conditions are applied at the midplane. Prior to mechanical loading, thermal residual stress development in the laminate due to cure shrinkage is modelled by subjecting it to a temperature drop from 180˚C (final cure temperature) to 20˚C (room temperature). Tensile loading is then introduced, by applying equal and opposite velocities on the two edges of the laminate. The velocity magnitude is kept sufficiently small (0.2mm/sec) to keep

the simulation quasi-static and avoid any dynamic effects. The selective mass-scaling option available in Abaqus/Explicit is used with a minimum allowed time increment size of 1μsec, such that any element not able to meet this requirement during simulation is selectively mass-scaled. This is only done to expedite the overall computation and checked carefully so that it has minimal influence on the overall load-displacement response.

The simulation outcomes for tensile failure stress levels are plotted in Figure 6, together with experimental results for the same. Clearly, the present approach matches the experiments very well. However, a conventional CDM under-predicts the strength by approximately 19% with respect to the experimental mean and lies outside the scatter band. The reason for this is clear from Figure 7, where the matrix cracks in the plies and delamination patterns in the ply interfaces just after failure are compared between the two approaches. The matrix cracks are more discrete and follow the fibre orientation in the current approach, as expected, while the conventional CDM results in diffused damage development over a large area in all the plies. More importantly, this diffuse nature of ply damage is not fully able to initiate and interact with delaminations, resulting in underdeveloped +45/90 and 90/-45 delaminations and erroneously formed -45/0 delamination. Due to better representation of matrix cracks, this problem is not present in the newly presented directed CDM approach, and results in very realistic delamination patterns (compared to experimental results from[41]), leading to an overall accurate failure stress prediction. The situation of incorrect crack and delamination interaction in the conventional CDM method also leads to spurious delamination and overall instability. To show this point more clearly, in Figure 8 the delamination pattern evolution in the +45/90 interface is compared between the two methods, together with the matrix crack development in the adjoining plies at different stress levels during loading. The conventional CDM method leads to premature delamination due to widespread diffused damage in the 90˚

ply (shown in grey). The delamination on either side of the hole does not develop to its full extent, instead the model fails unstably at a much lower overall tensile stress level. This is not the case with directed CDM method, where the sharp matrix cracks are able to initiate and develop triangular delamination patterns at either side of the hole, providing better numerical stability to the model and causing failure at a stress level that agrees with the experiment.

Another important aspect of modelling failure of open-hole specimens is the ability to correctly represent the axial stress redistribution in the 0˚ ply near the hole due to splitting. The importance of this has been discussed in [43]. Relaxation of the axial stress due to formation and growth of splits (here directed CDM cracks in 0˚ plies) is verified by plotting the variation of axial stress in an element near the hole (see Figure 9) as a function of the split length. This clearly shows that the method is able to reproduce the stress relaxation in the 0˚ plies due to split formation prior to delamination propagation.

The second layup modelled is $[90_2/-45_2/0_2/45_2]_S$, with the model preparation and load application remaining exactly same as the previous layup. The outcome of this model is only briefly discussed here since the quality of comparison to experiments from [42] is very similar to the first layup presented above. In this case, the amount of delamination is less that in the first layup and therefore the failure stress increases to a higher value. The delamination pattern at failure in the different interfaces predicted by the directed CDM matches closely with that reported in [42], modelled using individual matrix cracks explicitly embedded in the mesh pattern. The predicted failure stress from [42] is 512 MPa and experimental strength is 499MPa. The directed CDM method predicts failure at 502 MPa, thus confirming the robustness of the present method.

3.2 Static tensile failure of un-notched quasi-isotropic laminate

Hallett *et al.*[18] have also previously investigated the unnotched tensile strength of the same $[45_2/90_2/-45_2/0_2]$s laminates. The failure in this case is not delamination-driven, but due to fibre rupture in the 0˚ plies. Modelling work in [18] showed that matrix crack development in the -45˚ plies cause local stress concentrations in the adjoining 0 plies, which leads to 0° plies failing with a fracture surface aligned with the -45° fibre direction. The numerical models in [18]used a fibre-aligned mesh with cohesive elements pre-inserted between and within plies to simulate delamination and matrix cracking respectively. Although, no fibre failure was explicitly modelled, highly localised axial stresses, which exceeded the material tensile strength, were observed in the contour plot of 0˚ plies, in a region immediately adjacent to a -45˚ ply matrix crack, thus confirming this mechanism of failure.

The new directed CDM method is here tested as to whether the above-mentioned matrix crack-fibre failure interaction could be captured well. Only the specimen gauge length is modelled for faster computation and a 0.25 mm×0.25 mm mesh is used in the region of interest (Figure 10). The 0˚ ply axial stress contour is checked and the simulation is discontinued when the axial stress exceeds the volume dependent unidirectional fibre strength (2687 MPa for a volume similar to only 0°plies in the laminate, for the material system in Table 1[18]).

The contour plot of the axial stress in the 0˚ ply is shown in Figure 11, for the present and conventional CDM approaches respectively, when the laminate cross-sectional stress reaches 645 MPa. The axial stress concentrations along the -45° crack line, which exceeds the material strength at this point are clearly visible in Figure 11 (top). This also agrees well with the experimental failure stress 660 MPa (3.3% C.V)[18]. In contrast the only stress concentrations in the conventional CDM are near the boundary conditions as shown in Figure 11 (bottom), with a stress level much below that required for fibre. Figure 12 shows the

discretely represented multiple cracks in different plies at failure. The same is not observed for the conventional CDM approach, where in the absence of a predefined stress concentration such as the open hole in section 3.1, matrix cracks in the off-axis plies were seen to be even more diffuse. These smeared matrix cracks are unable to cause localisation of the stresses in adjacent plies and could not capture the damage interaction between cracks and fibre failure. In this case, the simulation finally ended unstably due widespread damage causing element distortion.

4 Conclusion

The problem of mesh pattern sensitivity in composite damage modelling using traditional continuum damage models is highlighted and overcome in this work. A ply based crack tracking approach is suggested as an additional capability on top of any standard continuum damage model and with any given FE mesh pattern, with minimal computational overhead. Two challenging test cases are demonstrated in the present study clearly showing the superiority of this method over traditional CDM, both in terms of accuracy and numerical stability while modelling complex progressive failure of multidirectional laminates. In these cases, the discrete representation of individual matrix cracks and their correct orientation within a ply is quite crucial, as they interact with other damage mechanisms during failure. The quality of results is similar to other more established methods for introducing discrete matrix cracks, such as XFEM or oriented meshes, but the computational and pre-processing complexity is greatly reduced. With XFEM-like methods several additional complexities arise, such as the need to partition elements to integrate discontinuous fields, additional memory management schemes in the programme to introduce and update additional nodes/degrees of freedom corresponding to the crack segments etc. Such complexities are not present in the current method. The full potential of the method could be harnessed in the

future for modelling of complex failure of structural scale components, where a crack oriented mesh construction is not an option. The method could also be extended to study dynamic failure, such as impact, where numerical stability can be an issue when using with traditional CDM methods.

5 References

[1] Kachanov L. Time of the rupture process under creep conditions. Izv Akad Nauk SSSR, Otd Tekhnicheskich Nauk 1958;8:26–31.

[2] Rabotnov YN. Creep rupture. 12th Int. Congr. Appl. Mech., Stanford: 1968.

[3] Leckie FA, Hayhurst DR. Creep Rupture of Structures. Proc R Soc London Ser A, Math Phys Sci 1974;340:323–47. doi:10.1098/rspa.1974.0155.

[4] Chaboche J .L. Le Concept de Contrainte Effective Appliqué à l'Élasticité et à la Viscoplasticité en Présence d'un Endommagement Anisotrope. In: Boehler J.P., editor. Mech. Behav. Anisotropic Solids, Springer, Dordrecht; 1982, p. 737–60.

[5] Lemaitre J. Evaluation of dissipation and damage in metals submitted to dynamic loading. Int. Conf. Mech. Behav. Mater., 1971, p. 540–9.

[6] Ladeveze P, Ledantec E. Damage modelling of the elementary ply for laminated composites. Compos Sci Technol 1992;43:257–67.

[7] Pinho ST, Iannucci L, Robinson P. Physically based failure models and criteria for laminated fibre-reinforced composites with emphasis on fibre kinking. Part I: Development. Compos Part A Appl Sci Manuf 2006;37:63–73.

[8] Pinho ST, Iannucci L, Robinson P. Physically based failure models and criteria for laminated fibre-reinforced composites with emphasis on fibre kinking. Part II: FE implementation. Compos Part A Appl Sci Manuf 2006;37:766–77. doi:10.1016/j.compositesa.2005.06.008.

[9] Maimí P, Camanho PP, Mayugo J a., Dávila CG. A continuum damage model for composite laminates: Part I - Constitutive model. Mech Mater 2007;39:897–908. doi:10.1016/j.mechmat.2007.03.005.

[10] Maimí P, Camanho PP, Mayugo J a., Dávila CG. A continuum damage model for composite laminates: Part II - Computational implementation and validation. Mech Mater 2007;39:909–19. doi:10.1016/j.mechmat.2007.03.006.

[11] Maimi P, Mayugo J a., Camanho PP. A Three-dimensional Damage Model for Transversely Isotropic Composite Laminates. J Compos Mater 2008;42:2717–45. doi:10.1177/0021998308094965.

[12] Williams K V., Vaziri R. Application of a damage mechanics model for predicting the impact response of composite materials. Comput Struct 2001;79:997–1011. doi:10.1016/S0045-7949(00)00200-5.

[13] Van Der Meer FP, Sluys LJ. Continuum Models for the Analysis of Progressive Failure in Composite Laminates. J Compos Mater 2009;43:2131–56. doi:10.1177/0021998309343054.

[14] Bazant, Zdenek P, Belytschko T. Wave propagation in a strain-softening bar: exact solution. J Eng Mech 1985;111:381–9.

[15] Bazant ZP. Crack band theory for fracture of concrete. Mater Struct 1983;16:155–77.

[16] Bazant ZP, Oh BH. Microplane model for progressive fracture of concrete and rock. J Eng Mech 1985;111:559–82.

[17] Maimí P, Mayugo JA, Camanho PP. A Three-dimensional Damage Model for Transversely Isotropic Composite Laminates. J Compos Mater 2008;42:2717–45. doi:10.1177/0021998308094965.

[18] Hallett SR, Jiang WG, Khan B, Wisnom MR. Modelling the interaction between matrix cracks and delamination damage in scaled quasi-isotropic specimens. Compos Sci Technol 2008;68:80–9. doi:10.1016/j.compscitech.2007.05.038.

[19] Wisnom MR, Khan B, Hallett SR. Size effects in unnotched tensile strength of unidirectional and quasi-isotropic carbon/epoxy composites. Compos Struct 2008;84:21–8. doi:10.1016/j.compstruct.2007.06.002.

[20] Pernice MF, De Carvalho N V., Ratcliffe JG, Hallett SR. Experimental study on delamination migration in composite laminates. Compos Part A Appl Sci Manuf 2015;73:20–34. doi:10.1016/j.compositesa.2015.02.018.

[21] Nikishkov Y, Makeev A, Seon G. Finite Element-Based Simulation of Damage in Composites. J Am Helicopter Soc 2009;55:9. doi:10.1017/CBO9781107415324.004.

[22] Song K, Li Y, Rose C a. Continuum Damage Mechanics Models for the Analysis of Progressive Failure in Open-Hole Tension Laminates. Am Inst Aeronaut Astronaut 2011:1–18. doi:10.2514/6.2011-1861.

[23] Lopes CS, Sádaba S, González C, Llorca J, Camanho PP. Physically-sound simulation of low-velocity impact on fiber reinforced laminates. Int J Impact Eng 2016;92:3–17. doi:10.1016/j.ijimpeng.2015.05.014.

[24] Jiang WG, Hallett SR, Green BG, Wisnom MR. A concise interface constitutive law for analysis of delamination and splitting in composite materials and its application to scaled notched tensile specimens. Int J Numer Methods Eng 2007;69:1982–95. doi:10.1002/nme.

[25] Li X, Hallett SR, Wisnom MR. Numerical investigation of progressive damage and the effect of layup in overheight compact tension tests. Compos Part A Appl Sci Manuf 2012;43:2137–50. doi:10.1016/j.compositesa.2012.03.002.

[26] Sun XC, Wisnom MR, Hallett SR. Interaction of inter- and intralaminar damage in scaled quasi-static indentation tests: Part 2 - Numerical simulation. Compos Struct 2016;136:727–42. doi:10.1016/j.compstruct.2015.09.062.

[27] Serra J, Bouvet C, Castanié B, Petiot C. Scaling effect in notched composites : The Discrete Ply Model approach 2016;148:127–43. doi:10.1016/j.compstruct.2016.03.062.

[28] Forghani A, Vaziri R. Computational Modeling of Damage Development in Composite Laminates Subjected to Transverse Dynamic Loading. J Appl Mech 2009;76:51304. doi:10.1115/1.3129705.

[29] Jirásek M. Nonlocal models for damage and fracture: Comparison of approaches. Int J Solids Struct 1998;35:4133–45. doi:10.1016/S0020-7683(97)00306-5.

[30] Cahill LMA, Natarajan S, Bordas SPA, O'Higgins RM, McCarthy CT. An

experimental/numerical investigation into the main driving force for crack propagation in uni-directional fibre-reinforced composite laminae. Compos Struct 2014;107:119–30. doi:10.1016/j.compstruct.2013.05.039.

[31] Ebrahimi SH, Mohammadi S, Asadpoure A. An Extended Finite Element (XFEM) Approach for Crack Analysis in Composite Media. Int J Civ Eng 2008;6:198–207.

[32] Iarve EV, Gurvich M., MollenHauer DH, Rose C., Dávila C. Mesh-independent matrix cracking and delamination modeling in laminated composites. Int J Numer Methods Eng 2011:749–73.

[33] Van Der Meer FP, Sluys LJ. A phantom node formulation with mixed mode cohesive law for splitting in laminates. Int J Fract 2009;158:107–24. doi:10.1007/s10704-009-9344-5.

[34] Chen BY, Pinho ST, De Carvalho N V., Baiz PM, Tay TE. A floating node method for the modelling of discontinuities in composites. Eng Fract Mech 2014;127:104–34. doi:10.1016/j.engfracmech.2014.05.018.

[35] Ling D, Yang Q, Cox B. An augmented finite element method for modeling arbitrary discontinuities in composite materials. Int J Fract 2009;156:53–73. doi:10.1007/s10704-009-9347-2.

[36] Liu W, Yang QD, Mohammadizadeh S, Su XY. An efficient augmented finite element method for arbitrary cracking and crack interaction in solids. Int J Numer Methods Eng 2014:438–68.

[37] Remmers JJC, De Borst R, Needleman a. A cohesive segments method for the simulation of crack growth. Comput Mech 2003;31:69–77. doi:10.1007/s00466-002-0394-z.

[38] Kawashita LF, Bedos A, Hallett SR. Modelling mesh independent transverse cracks in laminated composites with a simplified cohesive segment method. C Mater Contin 2012;32:133–58.

[39] Abaqus Inc. Abaqus 6.14 documentation. Providense,RI,USA: 2014.

[40] Hallett SR, Green BG, Kin WJ, Cheung H, Wisnom MR. The open hole tensile test : a challenge for virtual testing of composites. Int J Fract 2009;158:169–81. doi:10.1007/s10704-009-9333-8.

[41] Green BG, Wisnom MR, Hallett SR. An experimental investigation into the tensile strength scaling of notched composites 2007;38:867–78. doi:10.1016/j.compositesa.2006.07.008.

[42] Hallett SR, Jiang WG, Wisnom MR. Effect of Stacking Sequence on Open-Hole Tensile Strength of Composite Laminates. Am Inst Aeronaut Astronaut 2009;47. doi:10.2514/1.41244.

[43] Iarve E V, Mollenhauer D, Kim R. Theoretical and experimental investigation of stress redistribution in open hole composite laminates due to damage accumulation. Compos Part A Appl Sci Manuf 2005;36:163–71. doi:10.1016/j.compositesa.2004.06.011.

[44] Pinho ST, Darvizeh R, Robinson P, Schuecker C. Material and structural response of polymer-matrix fibre-reinforced composites 2012. doi:10.1177/0021998312454478.

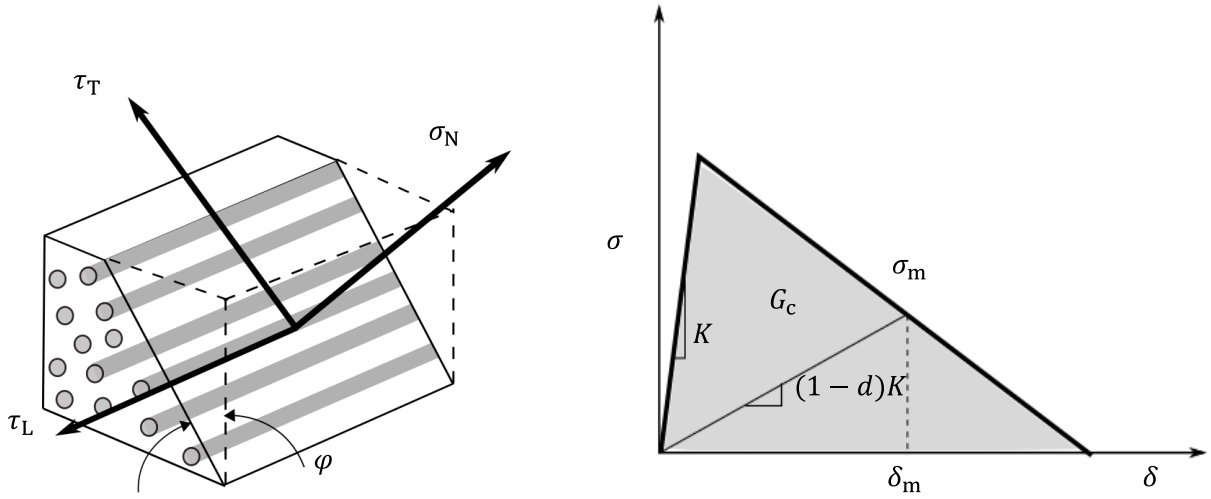

(a) (b)

Figure 1.(a) Matrix crack plane and associated traction components (b) Bilinear cohesive damage law.

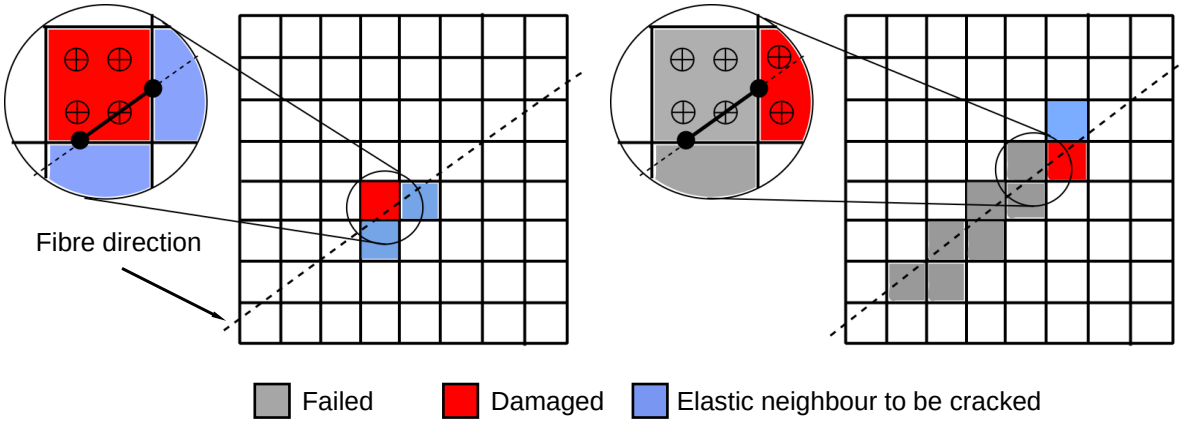

(a) (b)

Figure 2. (a) Crack passing through an integration point in absence of a failed neighbour (b) Crack coming from an already failed element and passing independently of the integration point location to maintain advancement along fibre direction.

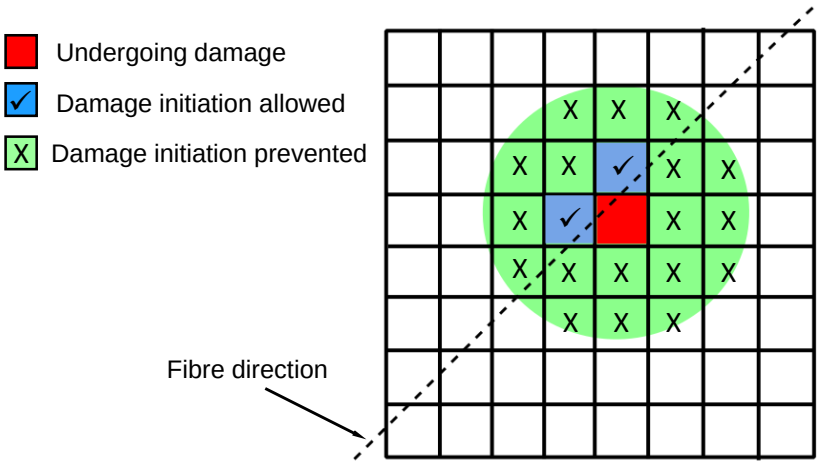

Figure 3. Artificial blocking of crack initiation within a user-defined circular region

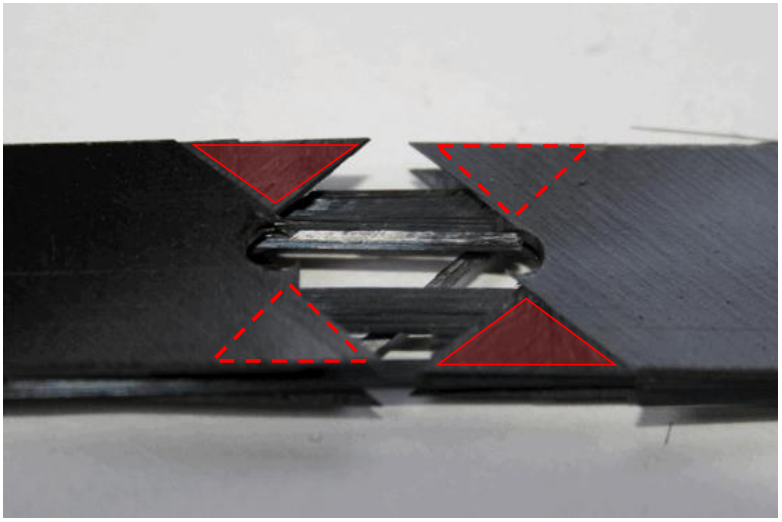

Figure 4. Triangular delamination pattern highlighted in red (visible area by solid lines, and non-visible by dashed lines) in a quasi-isotropic open-hole specimen failed in tension.

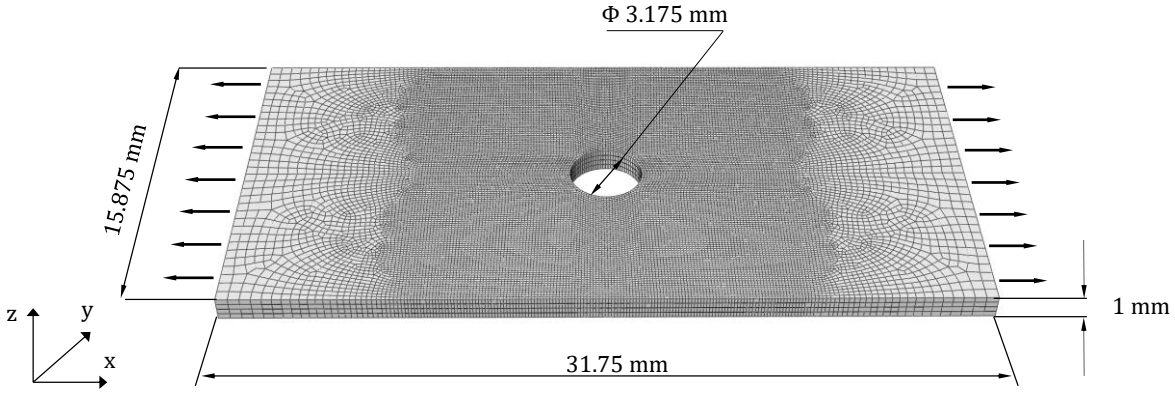

Figure 5. FE mesh of the open-hole specimen (only the gauge length is modelled for computational efficiency)

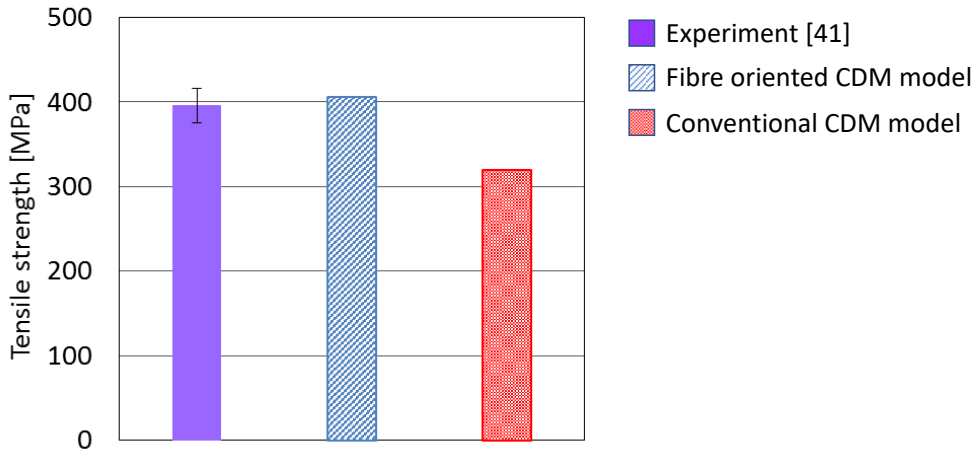

Figure 6. Failure stresses obtained from the present and conventional CDM approaches, compared experiment for open hole tensile failure of a$[45_2/90_2/-45_2/0_2]_S$ laminate.

Conventional CDM		Directed CDM	
Matrix cracks	Delamination	Matrix cracks	Delamination
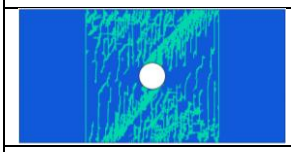	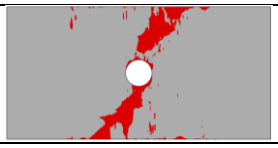	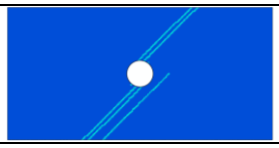	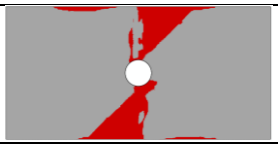
+45° ply	+45/90 Interface	45° ply	+45/90 Interface
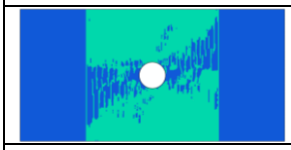	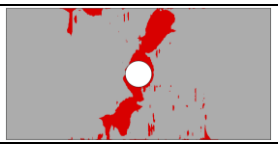	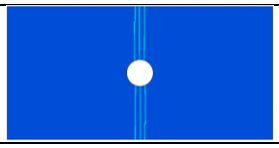	
90° ply	90/-45 interface	90° ply	90/-45 interface
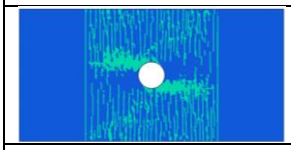	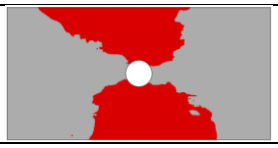	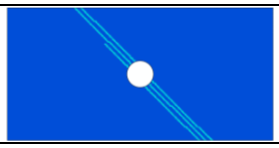	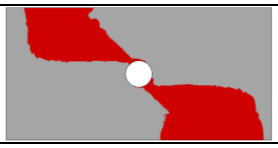
-45° ply	-45/0 interface	-45° ply	-45/0 interface
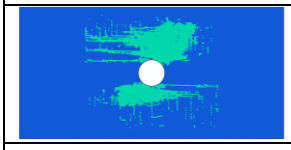		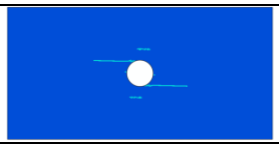	
0° ply		0° ply	

Figure 7.Damage profile obtained from simulations with ply matrix cracks shown in turquoise and inter-ply delaminations shown in red

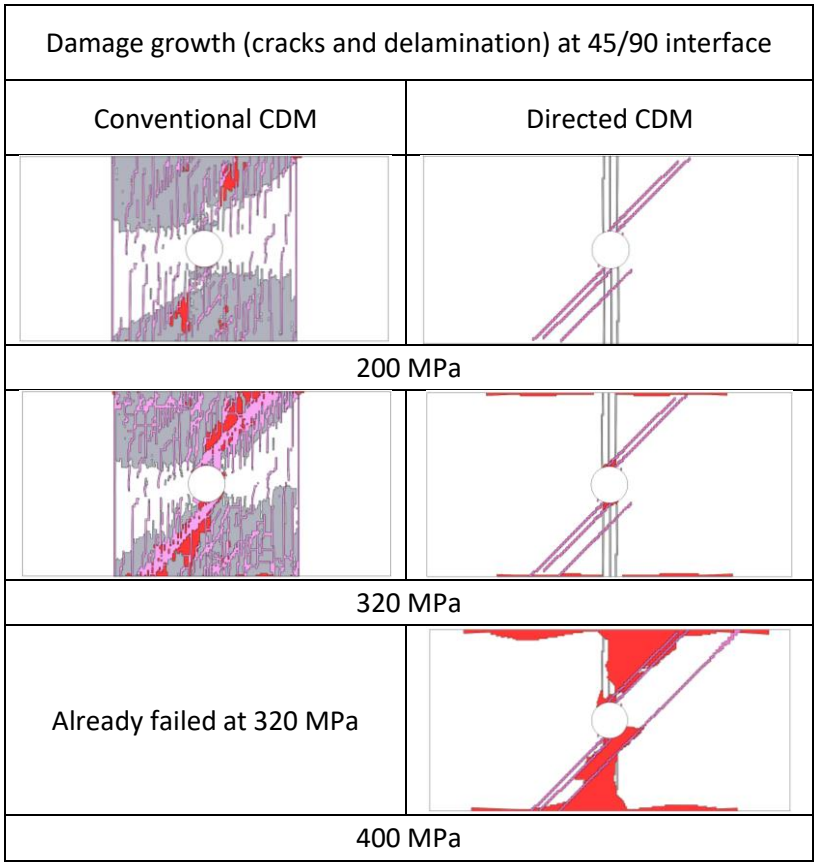

Figure 8. Interaction of matrix cracks (+45˚ ply cracks shown in pink and 90˚ ply cracks in grey) with delamination (shown in red) at the +45/90 interface with applied loading, compared between the conventional and directed CDM method.

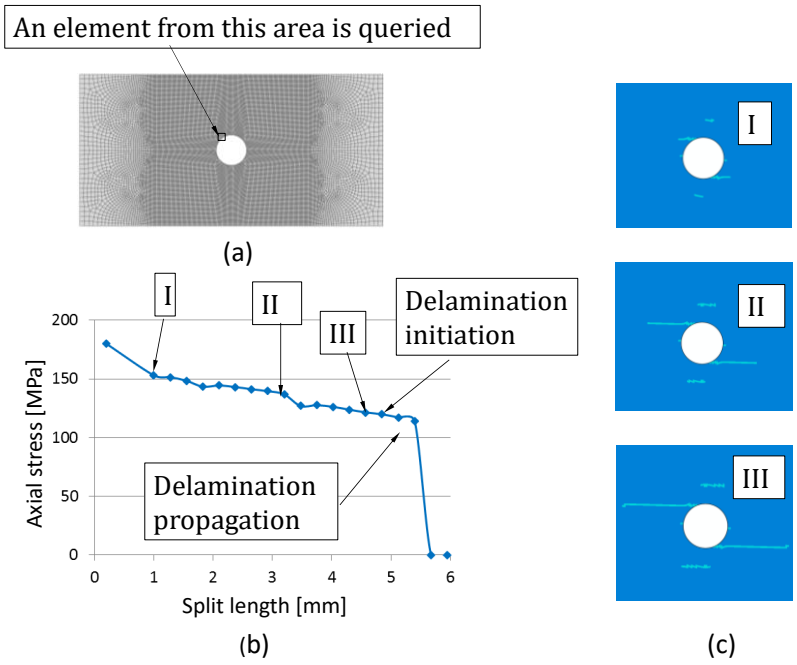

Figure 9. Axial stress relaxation near the hole in the 0˚ ply. (a) Location of the element from where the axial stress is recorded (b) Axial stress vs. split length during three stages of the split growth (shown in turquoise) corresponding to (c).

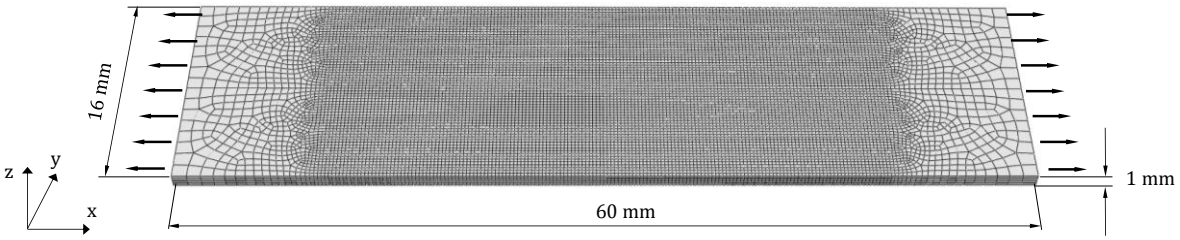

Figure 10. FE mesh of the unnotched quasi-isotropic specimen.

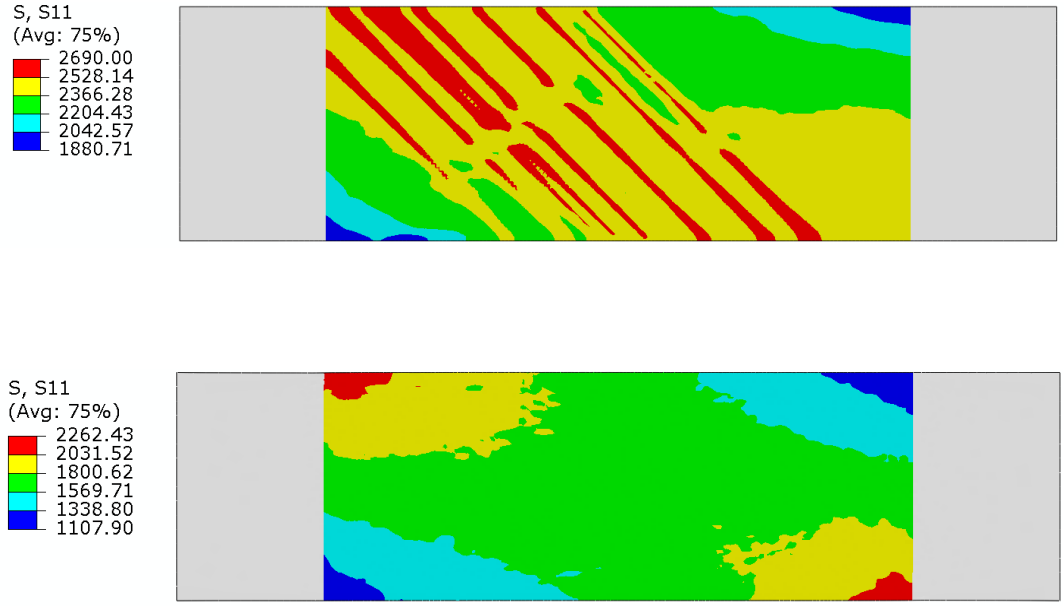

Figure 11. Contour plot of axial stress in the 0° ply in directed CDM (top) and conventional CDM (bottom), at the same cross-sectional stress level. In the directed CDM method, 0° ply already failed due to matrix crack induced local stress concentration. In conventional method, the ply remains undamaged at this point.

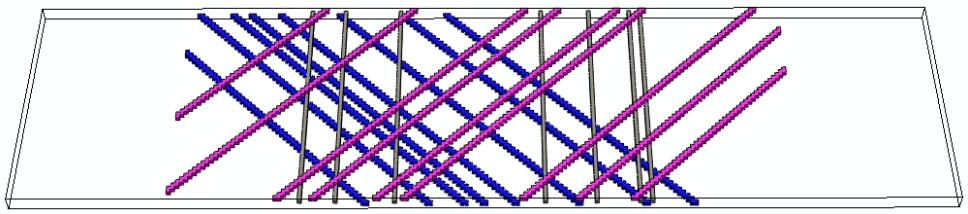

Figure 12.Overall pattern of matrix crack development inside the laminate at failure: 45˚ cracks (pink), -45˚ cracks (blue) and 90˚ cracks (grey).

Table 1. Material properties of IM7/8552[18,44]

E_{11}	E_{22}	E_{33}	ν_{12}	ν_{13}	ν_{23}	G_{12}	G_{13}	G_{23}	α_{11}	α_{22}	α_{33}
(MPa)	(MPa)	(MPa)				(MPa)	(MPa)	(MPa)	(/°C)	(/°C)	(/°C)
161000	11380	11380	0.32	0.32	0.43	5170	5170	3980	0	3e-5	3e-5

Y_T	Y_c	S_L	G_{Ic}	G_{IIc}	α
(MPa)	(MPa)	(MPa)	(N/mm)	(N/mm)	
60	185	90	0.2	1.0	1.0

Table 2. Cohesive interface properties [18]

K_I (N/mm^3)	K_{II} (N/mm^3)	σ_I^{max} (MPa)	σ_{II}^{max} (MPa)	G_{Ic} (N/mm)	G_{IIc} (N/mm)	α (-)
10^5	10^5	60	90	0.2	1.0	1